The Journal of Infectious Diseases
SUPPLEMENT ARTICLE

Evaluating the Performance of Pathogen-Targeted Positron Emission Tomography Radiotracers in a Rat Model of Vertebral Discitis-Osteomyelitis

Matthew F. L. Parker,[1,2] Marina López-Álvarez,[1] Aryn A. Alanizi,[1] Justin M. Luu,[1] Ilona Polvoy,[1] Alexandre M. Sorlin,[1] Hecong Qin,[1] Sanghee Lee,[1] Sarah J. Rabbitt,[1] Priamo A. Pichardo-González,[1] Alvaro A. Ordonez,[3] Joseph Blecha,[1] Oren S. Rosenberg,[4] Robert R. Flavell,[1] Joanne Engel,[4,5] Sanjay K. Jain,[3] Michael A. Ohliger,[1,6] and David M. Wilson[1]

[1]Department of Radiology and Biomedical Imaging, University of California, San Francisco; [2]Department of Psychiatry, Renaissance School of Medicine at Stony Brook University, New York; [3]Center for Infection and Inflammation Imaging Research, Department of Pediatrics, Johns Hopkins University School of Medicine, Baltimore, Maryland; [4]Department of Medicine, University of California, San Francisco; [5]UCSF Department of Microbiology and Immunology, San Francisco, California; and [6]Department of Radiology, Zuckerberg San Francisco General Hospital, San Francisco, California

Background. Vertebral discitis-osteomyelitis (VDO) is a devastating infection of the spine that is challenging to distinguish from noninfectious mimics using computed tomography and magnetic resonance imaging. We and others have developed novel metabolism-targeted positron emission tomography (PET) radiotracers for detecting living Staphylococcus aureus and other bacteria in vivo, but their head-to-head performance in a well-validated VDO animal model has not been reported.

Methods. We compared the performance of several PET radiotracers in a rat model of VDO. [^{11}C]PABA and [^{18}F]FDS were assessed for their ability to distinguish *S aureus*, the most common non-tuberculous pathogen VDO, from *Escherichia coli*.

Results. In the rat *S aureus* VDO model, [^{11}C]PABA could detect as few as 10^3 bacteria and exhibited the highest signal-to-background ratio, with a 20-fold increased signal in VDO compared to uninfected tissues. In a proof-of-concept experiment, detection of bacterial infection and discrimination between *S aureus* and *E coli* was possible using a combination of [^{11}C]PABA and [^{18}F]FDS.

Conclusions. Our work reveals that several bacteria-targeted PET radiotracers had sufficient signal to background in a rat model of *S aureus* VDO to be potentially clinically useful. [^{11}C]PABA was the most promising tracer investigated and warrants further investigation in human VDO.

Keywords. Infection imaging; metabolism; nuclear medicine; *S aureus*; positron emission tomography.

Vertebral discitis-osteomyelitis (VDO) is a common and potentially devastating infection, especially in patients who are immunocompromised, are intravenous drug users, or have other risk factors for hematogenous spread of infection [1]. The most common nontuberculous cause of VDO in patients is *Staphylococcus aureus*, a gram-positive bacterium whose management has been challenged by the emergence of multidrug-resistant strains such as methicillin-resistant *S aureus* (MRSA) [2]. Not only can uncontrolled infection lead to sepsis, but abscess formation and granulation tissue can occupy the epidural space, leading to compression of the spinal cord. The diagnosis of VDO is difficult in both the acute and chronic setting and may present as a indolent disease, especially in older patients [3]. The current diagnostic gold standard requires invasive tissue sampling, Gram staining, and a positive culture to definitively diagnose infection and to determine antibiotic susceptibilities to guide optimal therapy. However, given the location of the nerve roots and the lack of external landmarks, biopsies of the spine may be low yield [4] and even potentially dangerous for the patient. In the case of documented infection, institution of effective antibiotic therapy is associated with improved outcomes. In contrast, unnecessary antibiotic treatment has associated morbidity, including disruption of the microbiome and selection for antibiotic-resistant organisms [5, 6].

The symptoms of VDO can be nonspecific, with laboratory testing including white blood cell (WBC) count, C-reactive protein, and erythrocyte sedimentation rate frequently inconclusive [7]. Both computed tomography (CT) and magnetic resonance imaging (MRI) are used in the evaluation of VDO in addition to nuclear imaging techniques [8–11]. Current imaging techniques are limited in the accurate diagnosis of VDO, as CT and MRI both rely on the presence of nonspecific structural abnormalities that often occur late in the disease process and can mimic processes such as osteoradionecrosis, rheumatologic disease, or age-related degeneration [12, 13]. The evaluation of VDO, especially in chronic cases, would benefit greatly from an imaging approach that is highly specific to live bacteria, both for diagnosis and monitoring antibiotic response.

Correspondence: David Wilson, MD, PhD, Department of Radiology and Biomedical Imaging, University of California, San Francisco, 505 Parnassus Ave, San Francisco, CA 94143 (david.m.wilson@ucsf.edu).

The Journal of Infectious Diseases® **2023;228(S4):S281–90**

https://doi.org/10.1093/infdis/jiad159

Although many infections may be diagnosed using MRI and CT, it is frequently difficult to distinguish bacterial infection from noninfectious entities. Several nuclear imaging tools have been applied to this problem, in particular ^{111}In WBC scanning, in which the patient's own immune cells are radiolabeled and single-photon emission computed tomography (SPECT) is performed [14], and [^{67}Ga]gallium citrate scanning [15, 16] targeting the transferrin receptor and potentially bacterial siderophores [17]. Recently, the investigation of cardiovascular and other infections has included full-body positron emission tomography (PET) using 2-deoxy-2-[^{18}F]fluoroglucose ([^{18}F]FDG), the radiotracer widely used in oncologic imaging [18]. Like cancer cells, activated immune cells have increased glucose uptake and thus may be detected using FDG-PET. However, lack of specificity —for example, distinguishing infection from tumor—is a major problem for both SPECT and PET approaches. Furthermore, these imaging techniques are dependent on host inflammatory response, which may be reduced or absent in individuals with a compromised immune system, for example patients with human immunodeficiency virus/AIDS, or undergoing chemotherapy and thus at higher risk for infection [19].

To overcome these obstacles to precise identification of VDO and other infections, there has been a pronounced interest in developing methods to detect bacteria in vivo during active infection. Several imaging strategies have targeted diverse bacterial-specific metabolic pathways to yield fluorescent bacteria or, more recently, for PET imaging [20]. These approaches have included radiolabeled antibiotics, sugars, sugar alcohols, antibodies, and peptides, with some of the most promising approaches including 2-deoxy-2-[^{18}F]fluorosorbitol ([^{18}F]FDS) showing dramatic data in infected patients [21, 22]. In our laboratory, we have focused on PET-compatible D-amino acids including D-[methyl-^{11}C]methionine ([^{11}C]D-met) [23, 24] and D-[3-^{11}C]alanine ([^{11}C]D-ala [25], as well as the folate-targeted radiotracer α-[^{11}C]para-aminobenzoic acid ([^{11}C]PABA) [26, 27]. Based on published in vitro studies using *Staphylococcus aureus* (the most common causative organism in VDO [7, 28], we studied a VDO rat model [25, 29] using several bacteria-targeted PET radiotracers (Figure 1). We performed micro-PET-CT (μPET-CT) on infected animals, to show how dual-modality imaging (PET-CT or PET-MRI) might be applied to patients to not only identify the presence of infection, but spatially localize it. In combination with an anatomic imaging method, bacteria-targeted PET could be used to detect *S aureus* in multiple locations, for example within infected heart valves, prosthetic joints, and intervertebral discs.

MATERIALS AND METHODS

Radiotracer Syntheses

In all cases, PET radiotracers were synthesized as we have previously described. [^{11}C]PABA was synthesized from a commercially available Grignard precursor [26]. [^{11}C]D-ala was synthesized using symmetric alkylation of glycine-derived precursors via [^{11}C]methyl iodide, in the presence of a phase-transfer cinchonidinium catalyst [25]. [^{11}C]D-met was synthesized in-loop from a linear D-homocysteine precursor in >99% enantiomeric excess [24]. [^{68}Ga]gallium citrate was generated by eluting [^{68}Ga] from a Ge-68/Ga-68 Generator with trapping on a cartridge and subsequent elution via sodium citrate [25]. [^{18}F]FDG was synthesized by the University of California, San Francisco (UCSF) cyclotron facility using standard procedures [25], while [^{18}F]FDS was produced via 2-electron reduction of [^{18}F]FDG by sodium borohydride [21]. All tracers used had radiochemical purities >99% and radiochemical yields/molar activities similar (within 50%) to mean values previously reported.

Structure	Name and Mechanism
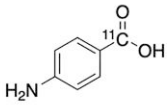	[^{11}C]para-aminobenzoic acid (PABA)
	Metabolite for folate synthesis
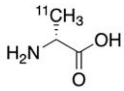	D-[^{11}C]alanine (D-Ala)
	Metabolite for peptidoglycan Synthesis
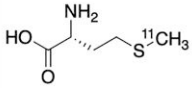	D-[^{11}C]methionine (D-Met)
	Metabolite for peptidoglycan synthesis
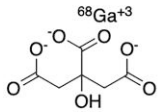	[^{68}Ga]gallium citrate (Ga-Cit)
	Inflammatory proteins (transferrin, lactoferrin); bacterial siderophores
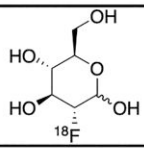	[^{18}F]fluoro-deoxyglucose (FDG)
	Metabolite for granulocytes present in areas of inflammation and for bacteria cells
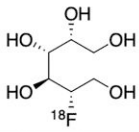	[^{18}F]fluoro-deoxysorbitol (FDS)
	Metabolic substrate for Enterobacteriaceae

Figure 1. Tracers employed in the rat vertebral discitis-osteomyelitis (VDO) model. The ^{11}C-labeled tracers [^{11}C]PABA, [^{11}C]D-ala, and [^{11}C]D-met were recently developed by our laboratories and have been shown to be sensitive to the strain of *Staphylococcus aureus* studied. Both [^{18}F]FDG and the single-photon emission computed tomography tracer [^{67}Ga]gallium citrate have been used clinically for decades, and applied to VDO, with the PET correlate [^{68}Ga]gallium citrate applied more recently to infected patients. The Enterobacteriaceae-sensitive [^{18}F]FDS has been studied in numerous preclinical models of infection and humans and is not significantly accumulated in *S aureus*.

Bacterial Strains and Growth Conditions

Bioluminescent *S aureus* Xen 29 (the strain studied throughout this work unless otherwise indicated) bacteria were aerobically grown in lysogeny broth (LB) containing 100 μg/L of kanamycin to an optical density at 600 nm of 1.0, followed by centrifugation and resuspension of the bacteria in an equal volume of 1× phosphate-buffered saline (PBS). Xen 29 is derived from the ATCC 12600 *S aureus* strain and possesses a stable copy of the *Photorhabdus luminescens* lux operon. Culture and preparation of *Escherichia coli* (ATCC 25922) was via an identical method, and heat-killed bacteria for all experiments were obtained using previously reported techniques [25].

Rat VDO Model

All animal procedures were approved by the UCSF Institutional Animal Care and Use Committee, and all studies were performed in accordance with UCSF guidelines regarding animal housing, pain management, and euthanasia. Sprague-Dawley rats (male, 10–12 weeks old, Charles River Laboratories) were used for all experiments. Rats were inoculated in the third intervertebral space with 50 μL of PBS containing 1.4×10^7 colony-forming units (CFU) live bacteria or a 10-fold higher dose of heat-killed bacteria [21] into the third/sixth intervertebral spaces from the base of the tail at 50% depth (based on the diameter of the tail) as described previously [29]. The rats were imaged at 2, 4, 6, 8, and 10 days using a Xenogen IVIS 50 instrument or Inveon μPET-CT (Siemens, Erlangen, Germany) following injection with a PET radiotracer.

Radiotracer Screening

Several cohorts (n = 5 for [^{11}C]PABA; n = 5 for [^{11}C]D-ala; n = 3 for the remaining tracers) were inoculated with *S aureus* in the third intervertebral space, and 10× heat-killed *S aureus* in the fifth intervertebral space. Intervertebral infection was confirmed by Xenogen IVIS 50, followed by μPET-CT at 4 days. Region of interest (ROI) analysis from PET images was used to compare tracer performance.

[^{11}C]PABA Dynamic Imaging

Three rats were inoculated with *S aureus* in the third intervertebral space as above, with intervertebral infection confirmed by Xenogen IVIS 50 at 2 days. This cohort was subsequently studied via [^{11}C]PABA μPET-CT at 2, 4, 6, and 10 days via ROI analyses as above.

Infection Burden Analysis

Rats (n = 3 per group) were inoculated with 50 μL PBS containing 10^6, 10^4, or 10^2 CFU *S aureus* in the third intervertebral space. The inoculum was confirmed by serial dilution and plating as described previously [25]. The animals were imaged by Xenogen IVIS 50 and [^{11}C]PABA μPET-CT at 4 days, and then euthanized. Spinal sections were isolated and counted using gamma counting (Hidex, Turku, Finland), followed by homogenization of the spinal sections in a small volume of 1× PBS. Serial dilutions of harvested tissues homogenates were plated on LB 1% agar plates to quantify bacterial burden.

Dual Imaging of S aureus *and* E coli*–Infected VDO*

Three rats were inoculated with 1.4×10^7 CFU *E coli* in the third intervertebral space and 1.4×10^7 CFU *S aureus* in the fifth intervertebral space. They were subsequently imaged using Xenogen IVIS 50 and a dual tracer imaging protocol at 4 days, whereby the rats were administered [^{11}C]PABA (t = 0), imaged by μPET-CT (t = 50 minutes), administered [^{18}F]FDS (t = 80 minutes), and imaged by μPET-CT (t = 200 minutes). ROI analysis from PET images was used to show uptake at the 2 injection sites by *E coli* and *S aureus*.

Imaging

Bioluminescence

Animals were imaged on a Xenogen IVIS 50 to confirm technically successful intervertebral inoculation of *S aureus*. In vivo bioluminescence imaging data are presented on a color-scale overlaid on a grayscale photograph of mice and displayed as radiance (photons/second/cm^2/steradian) within a circular ROI. Images were analyzed using Living Image software (PerkinElmer). Bioluminescence imaging was primarily used to establish technically successful inoculation for subsequent PET imaging, without explicit analysis or correlation to PET tracer uptake.

μPET-CT

The same general protocol was used for all studies. A tail vein catheter was placed in rats under isoflurane anesthesia. For carbon-11 studies, approximately 800 μCi of radiotracer was injected via the tail vein catheter. For [^{68}Ga]gallium citrate studies, approximately 250 μCi of [^{68}Ga]gallium citrate was injected via the tail vein catheter. For fluorine-18 studies, approximately 150 μCi of radiotracer was injected via the tail vein catheter. The animals were placed on a heating pad to minimize shivering. Mice were allowed to recover and micturate, and at the time points indicated (40 minutes for carbon-11 tracers, 120 minutes for fluorine-18 tracers, and 50 minutes/200 minutes for Gram staining), were placed back under isoflurane anesthesia. The animals were then transferred to the μPET-CT system and imaged using a single static 20-minute PET acquisition followed by a 10-minute micro-CT scan for attenuation correction and anatomical co-registration. No adverse events were observed during or after injection of any compound. Anesthesia was maintained during imaging using isoflurane. As described in the Results section, several cohorts were studied using ex vivo biodistribution analysis following completion of imaging and sacrifice. Gamma counting of harvested tissues was performed using a Hidex Automatic Gamma Counter as above.

Data Analysis and Statistical Methods

Both ROI and ex vivo biodistribution analyses were performed.

ROI Analysis

μPET-CT data were analyzed using the open source software AMIDE [30] and percent injected dose per cubic centimeter (%ID/cc) was used for quantitative comparison. %ID/cc values were established via 8 mm^3 ROIs using the elliptical tool.

Ex Vivo Analysis

Following some studies, the rats were killed and the spinal tissue was homogenized for Hidex gamma counting studies, and serial dilution (1× PBS) and plating to quantify the CFU present at the time of imaging.

Data Representation

All statistical analyses were performed using Prism software version 9.0 (GraphPad, San Diego, California). Live versus heat-killed comparisons were analyzed using paired *t* tests. Dynamic imaging data were analyzed using repeated-measures 1-way analysis of variance, followed by Tukey multiple comparison tests. Dose responses of [^{11}C]PABA uptake were analyzed using unpaired *t* tests. $P < .05$ was considered statistically significant. All graphs are depicted with error bars corresponding to the standard error of the mean.

Please see the Supplementary Materials and Methods for detailed information regarding microbiology, radiosynthesis, and several in vitro studies.

RESULTS

Bioluminescent Imaging of *S aureus* Xen 29-Infected Rats Reveal the Highest In Vivo Signals at 4 Days Postinfection in the Rat VDO Model

In this study, we used a previously published rat VDO model [29], in which we have previously examined the behavior of the bacterial metabolism-specific tracer [^{11}C]D-ala. The goal of using bioluminescent *S aureus* was to establish technically successful intervertebral inoculation for subsequent analysis using μPET-CT. Using a Xenogen IVIS 50 instrument, we performed a time course of *S aureus* infection using a strain transformed with a bioluminescent plasmid, Xen 29, by inoculating the third intervertebral space. As qualitative signals from bioluminescent *S aureus* were maximal at day 4 (Figure 2), we used this time point for subsequent imaging studies using PET. The subsequent loss of optical signal over time has been reported for bioluminescent *S aureus* in this model, which reflects proliferation of the wild-type *S aureus* over time in the absence of plasmid maintenance in vivo [29].

Performance of [^{11}C]PABA, [^{11}C]D-Ala, [^{11}C]D-Met, and [^{18}F]FDS in the Rat *S aureus* VDO Model as Assessed by PET

This study used several PET radiotracers targeting bacterial metabolism developed recently in our laboratories ([^{11}C]PABA, [^{11}C]D-ala, [^{11}C]D-met, [^{18}F]FDS) (Figure 1) and compared them to the established tracers [^{68}Ga]gallium citrate and [^{18}F]FDG. Rats were infected with live or 10-fold excess heat-killed *S aureus* in the third intervertebral disc space [25]. Following IVIS confirmation of infection, we performed μPET-CT using these 6 tracers and analyzed the data using 8-mm spherical ROIs on AMIDE [30] for quantitative comparison. The visual differences between animal groups were striking (Figure 3*A*), with significantly higher uptake for *S aureus* compared to a 10-fold excess of heat-killed *S aureus* for [^{11}C]PABA, [^{11}C]D-ala, [^{11}C]D-met, and [^{68}Ga]gallium citrate (Figure 3*B*; $P = .0001$, .0001, .0008, and .0098, respectively). In contrast, uptake of [^{18}F]FDG was similar for live and heat-killed *S aureus* ($P = .5900$), and there was no discernable uptake of [^{18}F]FDS by either live or heat-killed *S aureus*. The corresponding fold differences (Figure 3*C*) show that [^{11}C]PABA had the highest signal-to-noise ratio (ie, live/heat-killed ratio) in this model, approximately 23-fold.

Dynamic Imaging of Rat VDO Model Using [^{11}C]PABA-PET Shows Increasing Signals Over Time

We next performed a time course of [^{11}C]PABA in 3 rats per cohort inoculated in the third intervertebral disc space with *S aureus*. Serial μPET-CT revealed increasing PET signals over the period of 10 days ($P = .28$), as shown in Figure 4. In contrast, the bioluminescent signals decreased over time in this model, as reported previously [29]. ROI analysis (%ID/cc

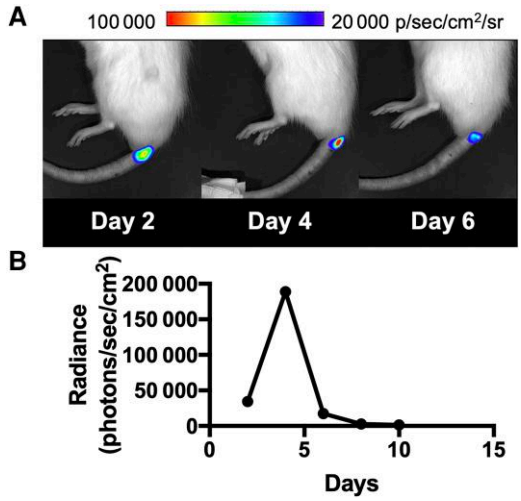

Figure 2. Optical imaging of the rat vertebral discitis-osteomyelitis model using bioluminescent *Staphylococcus aureus*. *A*, *S aureus* Xen 29 was inoculated at the third intervertebral space followed by serial imaging on a Xenogen IVIS 50 instrument as described in the Materials and Methods. Shown are representative bioluminescent signals at the site of inoculation on days 2, 4, and 6, indicative of technically successful intervertebral inoculation. *B*, Quantitative analysis of bioluminescent imaging performed at 2, 4, 6, 8, and 10 days demonstrates that day 4 is the optimal time for bioluminescent imaging of positron emission tomography tracers.

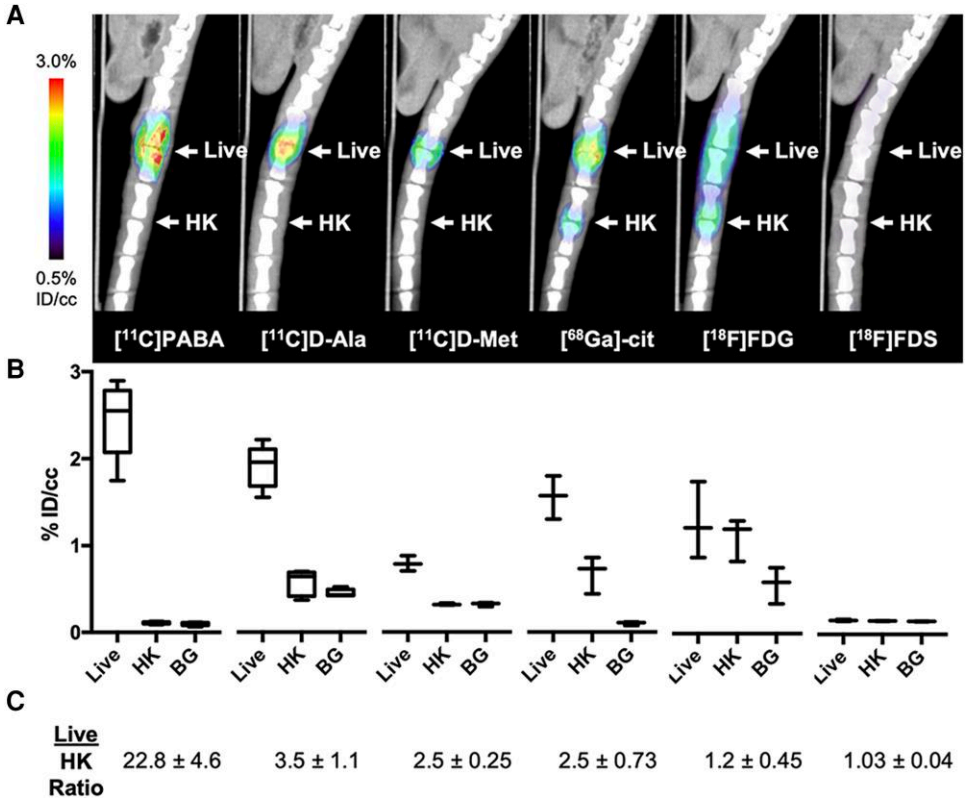

Figure 3. Performance of positron emission tomography (PET) tracers in the rat *Staphylococcus aureus* vertebral discitis-osteomyelitis (VDO) model at 4 days postinoculation. Rats were inoculated with *S aureus* (live) or a 10-fold excess of heat-killed (HK) bacteria in adjacent intervertebral spaces on day 0 with technically successful VDO infections confirmed using a Xenogen IVIS 50 instrument and studied using micro-positron emission tomography–computed tomography (μPET-CT) on day 4. *A*, μPET-CT imaging of infected rats (n = 5 for [^{11}C]PABA, n = 5 for [^{11}C]D-ala N = 3 for other tracers). PET signals at day 4 postinoculation were detected at the site of inoculation for all tracers except [^{18}F]FDS. *B*, Quantitative region of interest (ROI) analyses comparing inoculation of *S aureus*, 10-fold excess of HK *S aureus*, or background for the indicated tracers (background ROI was plotted for reference only). Statistically significant differences between live and HK levels were observed for [^{11}C]PABA ($P = .0003$, n = 5), [^{11}C]D-ala ($P = .0011$, n = 4), [^{11}C]D-met ($P = .0092$, n = 3), and [^{68}Ga]gallium citrate ($P = .0011$, n = 3), but not for [^{18}F]FDG ($P = .47$, n = 3). No [^{18}F]FDS uptake was observed for either live or HK *S aureus*. *C*, Ratio of live vs 10-fold excess of HK *S aureus* derived from ROI analyses of PET scans. Abbreviations: BG, background; HK, heat-killed; ID/cc, percent injected dose per cubic centimeter.

for comparison) showed that relative to day 2, [^{11}C]PABA had approximately 2.2-fold higher uptake on day 4 (adjusted $P = .015$), approximately 2.5-fold higher uptake on day 6 (adjusted $P = .086$), and approximately 2.9-fold higher uptake on day 10 ($P = .028$).

[^{11}C]PABA Uptake Is a Sensitive Probe of *S aureus* Infection in the Rat VDO Model

We investigated the limit of detection of *S aureus* via intervertebral inoculation decreasing inocula: 10^6, 10^4, or 10^2 CFU were inoculated, and the bacterial burden at the time of imaging was determined by homogenization, serial dilution and plating, with CFUs rounded to the nearest order of magnitude. We observed an approximately 10-fold increase for each of the inocula (10^7 10^5, and 10^3, respectively). μPET-CT imaging showed detectable [^{11}C]PABA accumulation at 3 doses (Figure 5*B*), which was further confirmed by ex vivo gamma counting (Supplementary Figure 1). Compared to PBS-inoculated segments, ROI analysis showed approximately 28-fold higher uptake ($P = .0001$) for 10^7 CFU, approximately 23-fold higher uptake ($P = .0001$) for 10^5 CFU, and approximately 6-fold higher uptake ($P = .0016$) for 10^3 CFU.

Simultaneous Detection of Gram-Positive and Gram-Negative Bacteria Using [^{11}C]PABA and [^{11}C]FDS

[^{18}F]FDS has been shown to be avidly and specifically taken up in vivo by gram-negative bacteria, with little or no uptake seen in gram-positive bacteria [21]. While this limits the utility of ^{18}F-FDS as the sole imaging tracer in the diagnosis of VDO, it does suggest the possibility of an in vivo "Gram stain" equivalent by simultaneously imaging with [^{11}C]PABA to detect both common gram-positive and gram-negative bacteria associated with VDO and with ^{18}F-FDS to detect gram-negative bacteria associated with VDO. To test this strategy, we employed the rat VDO model in which we inoculated *S aureus* into the third intervertebral space and *E coli* ATCC 25922 into the fifth intervertebral space. The animals were injected sequentially with 800 μCi of [^{11}C]PABA and imaged at

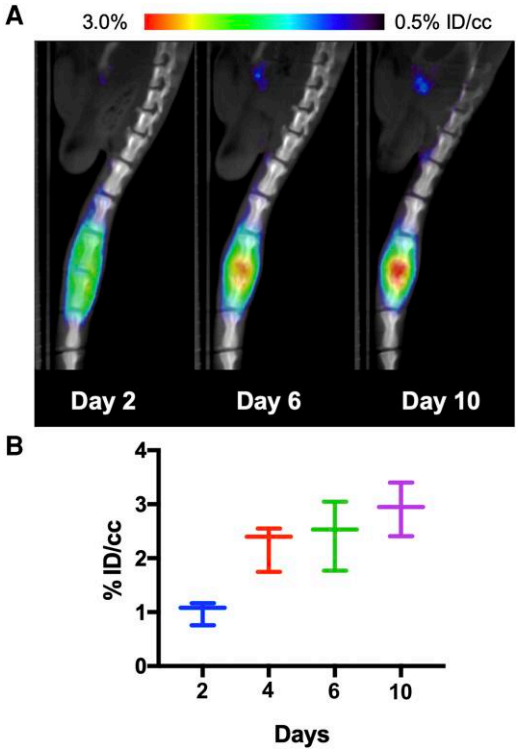

Figure 4. Dynamic study of [^{11}C]PABA in the rat vertebral discitis-osteomyelitis model. Mice were injected with [^{11}C]PABA on days 2, 4, 6, and 10 (n = 3 per cohort) after *Staphylococcus aureus* vertebral inoculation. *A*, Representative rat micro-positron emission tomography (PET)–computed tomography studies on days 2, 6, and 10. *B*, Graphical depiction of increasing PET signals over time. Abbreviation: ID/cc, percent injected dose per cubic centimeter.

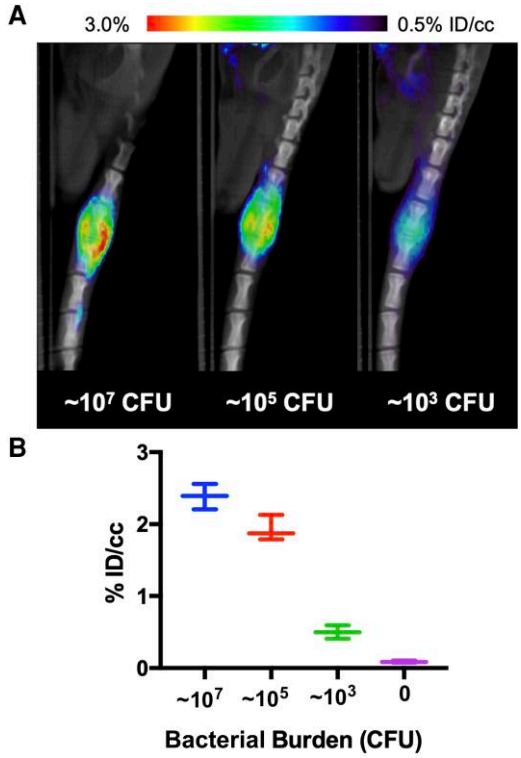

Figure 5. Dose response of [^{11}C]PABA uptake by *Staphylococcus aureus* in the rat vertebral discitis-osteomyelitis model. *A*, Cohorts of rats (n = 3 per group) were inoculated with either 10^2, 10^4, or 10^6 colony-forming units (CFU) *S aureus* and studied on day 4 using micro-positron emission tomography–computed tomography. The bacterial burdens were determined by homogenization of the spinal sections. *B*, Percent injeted dose per cubic centimeter (ID/cc) for each of the different inoculums and bacterial burdens. In all cases, infected intervertebral discs were compared to control (noninoculated rats) by region of interest analysis (10^7, ~28-fold, $P = .0001$; 10^5 ~23-fold, $P = .0001$; 10^3 ~6-fold, $P = .0016$).

t = 50 minutes, followed by administration of 150 μCi of [^{18}F]FDS at t = 80 minutes and imaging at 200 minutes (allowing carbon-11 decay). The total delay between the injection of [^{11}C]PABA and the initiation of [^{18}F]FDS imaging was approximately ten carbon-11 half-lives, making the radiotracer signal from the first scan noncontributory to the second scan. Subsequently, ROI analyses of the infected areas were performed for both time points. As shown in Figure 6, in *S aureus* infection, [^{11}C]PABA was retained but not [^{18}F]FDS. However, in an *E coli*–infected cohort, PET signals were detected using both [^{11}C]PABA and [^{18}F]FDS. These differences could be used to define both the location and to identify 2 different bacteria, at least for the *E coli* and *S aureus* strains used in this study.

DISCUSSION

Numerous PET and SPECT radiotracers have been used to study *S aureus* in vivo, including the clinical tracers [^{18}F]FDG and [^{67}Ga]gallium citrate in a rat VDO model [15, 31, 32]. More recently, several elegant approaches have been developed to improve the specificity of live *S aureus* detection. These include the use of sugars including 6′′-[^{18}F]-fluoromaltotriose [33, 34], which targets the bacterial maltose transport mechanism, and probes incorporated into the folate biosynthesis pathway, such as [^{18}F]fluoropropyl-trimethoprim [35] and [^{18}F]-labeled PABA derivatives [36]. Bacterial nitroreductase has been recently targeted for *S aureus* imaging, via both [^{18}F]PABA derivatives (using a nitro-prodrug) [37] and nitrogen mustard analogues [38]. Other diverse approaches use [^{68}Ga]-labeled bacterial siderophores (ie, desferrioxamine-B) [39], the host protein sphingosine-1-phosphate receptor 1 [40], the 6-position phosphorylated analogue of FDG [41], and the [^{99m}Tc]-labeled antimicrobial peptide ubiquicidin [42]. Some reports have also compared the performance of multiple tracers in preclinical models of *S aureus* infection [43, 44].

In our study, several PET tracers targeting bacterial metabolism ([^{11}C]PABA, [^{11}C]D-ala, [^{11}C]D-met) showed significant uptake compared to heat-killed bacteria in *S aureus* spinal infection, with [^{11}C]PABA showing the most promise

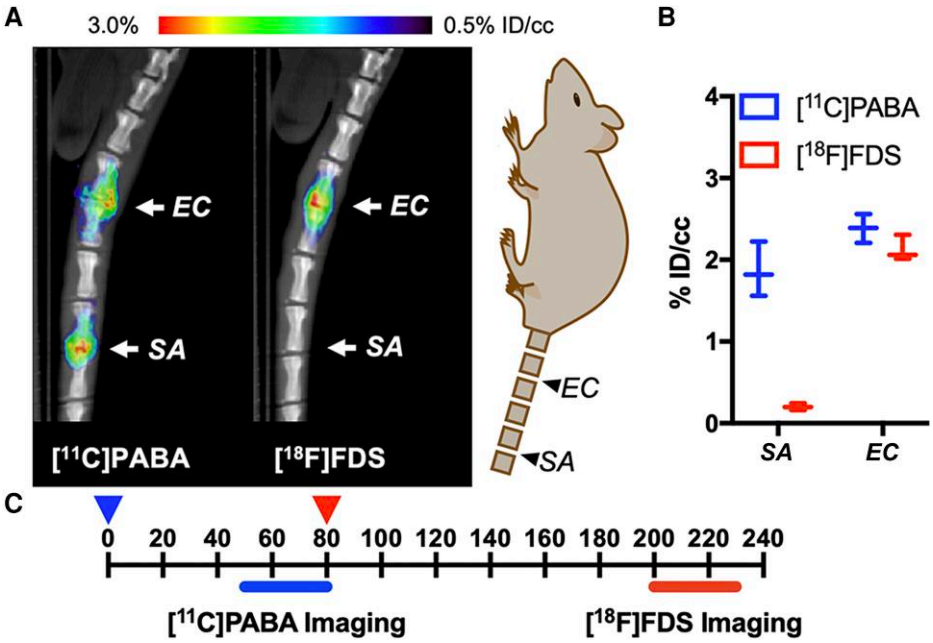

Figure 6. Comparison of [^{11}C]PABA and [^{18}F]FDS of rat vertebral discitis-osteomyelitis model of *Staphylococcus aureus* or *Escherichia coli* by micro-positron emission tomography–computed tomography (μPET-CT). *A*, [^{11}C]PABA and [^{18}F]FDS was serially administered to rats inoculated with both *S aureus* and *E coli* at different intervertebral segments on day 4 (n = 3), with μPET-CT subsequently performed. Both *S aureus* and *E coli* infections can be detected using [^{11}C]PABA, whereas only *E coli* can be detected using [^{18}F]FDS. *B*, Graphical depiction of data. *C*, Timeline for tracer injection and imaging time-points. Abbreviations: *EC*, *Escherichia coli*; ID/cc, percent injected dose per cubic centimeter; *SA*, *Staphylococcus aureus*.

given the high infection/background (>20-fold) ratio. We performed additional studies to suggest how the variable sensitivities of PET tracers might be leveraged in future clinical applications, for instance, in distinguishing gram-negative from gram-positive infections. For example, the more broadly sensitive [^{11}C]PABA could potentially be used in conjunction with the Enterobacteriaceae-targeted [^{18}F]FDS to identify broad classes of pathogens in vivo. We demonstrated the feasibility of this concept using *S aureus* Xen 29 and *E coli* ATCC 25922 in a small number of animals, but to be sufficiently robust in clinical practice, numerous additional data are needed. First, other bacterial causes of VDO need to be included in the analysis, for example, *Streptococcus pneumoniae*, *Enterococcus faecalis*, *Mycobacterium tuberculosis*, and *Salmonella* species. The PET tracer uptake of *Staphylococcus epidermidis* and other coagulase-negative staphylococci would be particularly important, since these (frequently commensal) organisms are often discovered in biopsy samples, confounding clinical management [45]. Finally, we and others have observed marked variability in PET tracer accumulation by multiple strains of the same species, for example, 2-deoxy-2-[^{18}F]fluoromannitol uptake by different *S aureus* clinical isolates [46]. Therefore, additional clinical strains of *S aureus* (including MRSA) and *E coli* should be investigated in the context of the described VDO model. Future preclinical analyses will include additional organisms and strains to better identify potential causes of false-negative and false-positive patient PET exams.

In addition to the incomplete set of pathogens studied, a major limitation of this study was the small number of animals used, necessitated by the rat VDO model, preclinical μPET-CT, and cyclotron use. Furthermore, we should emphasize that we sought a radiotracer that was sensitive to, rather than specific for, *S aureus*. The described approach cannot positively identify *S aureus* as a causative organism in vivo since numerous pathogens will accumulate [^{11}C]PABA or [^{11}C] D-ala. We do not have the techniques to identify individual species, and certainly not strains of a given species in vivo. In the future, these tools may be afforded by highly unique bacterial components (ie, *N*-acetyl muramic acid–related products in certain *Pseudomonas aeruginosa* strains [47]) or siderophore-mediated imaging strategies [48]. Finally, from a radiochemical standpoint, the use of the short $t_{1/2}$ [^{11}C]radionuclide presents a major obstacle to synthesizing and distributing PET tracers beyond the outpatient, academic setting. The discovery of new [^{18}F]-labeled tracers accumulated by *S aureus* is therefore critical for high clinical impact.

CONCLUSIONS

The goal of this study was to find a pathogen-targeted PET tracer that was sensitive to *S aureus* infection in a murine VDO model.

Several PET tracers targeting bacterial metabolism ([^{11}C]PABA, [^{11}C]D-ala, [^{11}C]D-met) showed significant uptake in *S aureus* spinal infection, with [^{11}C]PABA showing special promise given the high infection/background (>20-fold) ratio. The more broadly sensitive [^{11}C]PABA could potentially be used in conjunction with the Enterobacteriaceae-targeted [^{18}F]FDS to distinguish gram-positive from gram-negative infection in vivo.

Supplementary Data

Supplementary materials are available at *The Journal of Infectious Diseases* online. Consisting of data provided by the authors to benefit the reader, the posted materials are not copy-edited and are the sole responsibility of the authors, so questions or comments should be addressed to the corresponding author.

Notes

Author contributions. M. F. L. P., D. M. W., M. A. O., and S. K. J. proposed and supervised the overall project. M. F. L. P., J. B., H. Q., A. M. S., S. J. R., and S. L. performed or supported the radiochemistry. M. F. L. P., A. A. A., and J. M. L. developed the cell cultures for in vitro studies. M. F. L. P., A. M. S., H. Q., M. L.-A., P. A. P.-G., and I. P. performed the μPET-CT imaging studies, and M. F. L. P. and O. S. R. performed subsequent data analysis. M. F. L. P. and M. L.-A. performed ex vivo analysis. M. F. L. P., D. M. W., S. K. J., A. A. O., R. R. F., M. L.-A., H. Q., and J. E. wrote and edited the manuscript.

Financial support. This work was supported by the National Institutes of Health (grant numbers R01 EB024014, R01 EB025985, and R01 EB030897) and the Department of Defense (grant number DOD A132172).

Supplement sponsorship. This article appears as part of the supplement "Seeing Is Believing: The Potential of Molecular Imaging Approaches for Infectious Diseases," sponsored by the Center for Infectious Disease Imaging, Clinical Center, NIH (Intramural Research Program), and the Center for Infection and Inflammation Imaging Research, Johns Hopkins University School of Medicine, with individual contributions from Long Island Jewish Medical Center; University of California, San Francisco; and University of Maryland School of Pharmacy.

Potential conflicts of interest. The authors: No potential conflicts of interest.

All authors have submitted the ICMJE Form for Disclosure of Potential Conflicts of Interest. Conflicts that the editors consider relevant to the content of the manuscript have been disclosed.

References

1. Mylona E, Samarkos M, Kakalou E, Fanourgiakis P, Skoutelis A. Pyogenic vertebral osteomyelitis: a systematic review of clinical characteristics. Semin Arthritis Rheum **2009**; 39:10–7.
2. Purrello SM, Garau J, Giamarellos E, et al. Methicillin-resistant *Staphylococcus aureus* infections: a review of the currently available treatment options. J Glob Antimicrob Resist **2016**; 7:178–86.
3. Goel V, Young JB, Patterson CJ. Infective discitis as an uncommon but important cause of back pain in older people. Age Ageing **2000**; 29:454–6.
4. Sehn JK, Gilula LA. Percutaneous needle biopsy in diagnosis and identification of causative organisms in cases of suspected vertebral osteomyelitis. Eur J Radiol **2012**; 81:940–6.
5. Blaser M. Antibiotic overuse: stop the killing of beneficial bacteria. Nature **2011**; 476:393–4.
6. Khabbaz RF, Moseley RR, Steiner RJ, Levitt AM, Bell BP. Challenges of infectious diseases in the USA. Lancet **2014**; 384:53–63.
7. Gouliouris T, Aliyu SH, Brown NM. Spondylodiscitis: update on diagnosis and management. J Antimicrob Chemother **2010**; 65(Suppl 3):iii11–24.
8. Mazzie JP, Brooks MK, Gnerre J. Imaging and management of postoperative spine infection. Neuroimaging Clin N Am **2014**; 24:365–74.
9. Go JL, Rothman S, Prosper A, Silbergleit R, Lerner A. Spine infections. Neuroimaging Clin N Am **2012**; 22:755–72.
10. Talbott JF, Shah VN, Uzelac A, et al. Imaging-based approach to extradural infections of the spine. Semin Ultrasound CT MR **2018**; 39:570–86.
11. Polvoy I, Flavell RR, Rosenberg OS, Ohliger MA, Wilson DM. Nuclear imaging of bacterial infection: the state of the art and future directions. J Nucl Med **2020**; 61:1708–16.
12. Baker JC, Demertzis JL, Rhodes NG, Wessell DE, Rubin DA. Diabetic musculoskeletal complications and their imaging mimics. Radiographics **2012**; 32:1959–74.
13. Stacy GS, Kapur A. Mimics of bone and soft tissue neoplasms. Radiol Clin North Am **2011**; 49:1261–86. vii.
14. Palestro CJ. Radionuclide imaging of osteomyelitis. Semin Nucl Med **2015**; 45:32–46.
15. Hadjipavlou AG, Cesani-Vazquez F, Villaneuva-Meyer J, et al. The effectiveness of gallium citrate Ga 67 radionuclide imaging in vertebral osteomyelitis revisited. Am J Orthop **1998**; 27:179–83.
16. Lisbona R, Derbekyan V, Novales-Diaz J, Veksler A. Gallium-67 scintigraphy in tuberculous and nontuberculous infectious spondylitis. J Nucl Med **1993**; 34:853–9.
17. Emery T, Hoffer PB. Siderophore-mediated mechanism of gallium uptake demonstrated in the microorganism *Ustilago sphaerogena*. J Nucl Med **1980**; 21:935–9.
18. Gafter-Gvili A, Raibman S, Grossman A, et al. [^{18}F]FDG-PET/CT for the diagnosis of patients with fever of unknown origin. QJM **2015**; 108:289–98.

19. Dropulic LK, Lederman HM. Overview of infections in the immunocompromised host. Microbiol Spectr **2016**; 4. doi: 10.1128/microbiolspec.DMIH2-0026-2016
20. Parker MFL, Flavell RR, Luu JM, Rosenberg OS, Ohliger MA, Wilson DM. Small molecule sensors targeting the bacterial cell wall. ACS Infect Dis **2020**; 6:1587–98.
21. Weinstein EA, Ordonez AA, DeMarco VP, et al. Imaging Enterobacteriaceae infection in vivo with 18F-fluorodeoxysorbitol positron emission tomography. Sci Transl Med **2014**; 6:259ra146.
22. Ordonez AA, Wintaco LM, Mota F, et al. Imaging Enterobacterales infections in patients using pathogen-specific positron emission tomography. Sci Transl Med **2021**; 13:eabe9805.
23. Neumann KD, Villanueva-Meyer JE, Mutch CA, et al. Imaging active infection in vivo using D-amino acid derived PET radiotracers. Sci Rep **2017**; 7:7903.
24. Stewart MN, Parker MFL, Jivan S, et al. High enantiomeric excess in-loop synthesis of d-[methyl-11C]methionine for use as a diagnostic positron emission tomography radiotracer in bacterial infection. ACS Infect Dis **2020**; 6: 43–9.
25. Parker MFL, Luu JM, Schulte B, et al. Sensing living bacteria in vivo using D-alanine-derived 11C radiotracers. ACS Cent Sci **2020**; 6:155–65.
26. Mutch CA, Ordonez AA, Qin H, et al. [11c]para-aminobenzoic acid: a positron emission tomography tracer targeting bacteria-specific metabolism. ACS Infect Dis **2018**; 4:1067–72.
27. Ordonez AA, Parker MF, Miller RJ, et al. 11C-para-aminobenzoic acid PET imaging of *S. aureus* and MRSA infection in preclinical models and humans. JCI Insight **2022**; 7:e154117.
28. Dumont RA, Keen NN, Bloomer CW, et al. Clinical utility of diffusion-weighted imaging in spinal infections. Clin Neuroradiol **2019**; 29:515–22.
29. Bostian PA, Karnes JM, Cui S, et al. Novel rat tail discitis model using bioluminescent *Staphylococcus aureus*. J Orthop Res **2017**; 35:2075–81.
30. Loening AM, Gambhir SS. AMIDE: a free software tool for multimodality medical image analysis. Mol Imaging **2003**; 2:131–7.
31. Fragío-Gil JJ, González-Mazarío R, de la Rubia Navarro M, Román-Ivorra JA. The role of 18F-FDG PET/CT in early infectious discitis: a case report after a negative MRI. Radiol Case Rep **2019**; 14:1214–20.
32. Smids C, Kouijzer IJE, Vos FJ, et al. A comparison of the diagnostic value of MRI and 18F-FDG-PET/CT in suspected spondylodiscitis. Infection **2017**; 45:41–9.
33. Gowrishankar G, Hardy J, Wardak M, et al. Specific imaging of bacterial infection using 6″-18F-fluoromaltotriose: a second-generation PET tracer targeting the maltodextrin transporter in bacteria. J Nucl Med **2017**; 58:1679–84.
34. Wardak M, Gowrishankar G, Zhao X, et al. Molecular imaging of infective endocarditis with 6′′-[18F]fluoromaltotriose positron emission tomography-computed tomography. Circulation **2020**; 141:1729–31.
35. Sellmyer MA, Lee I, Hou C, et al. Bacterial infection imaging with [18F]fluoropropyl-trimethoprim. Proc Natl Acad Sci U S A **2017**; 114:8372–7.
36. Zhang Z, Ordonez AA, Wang H, et al. Positron emission tomography imaging with 2-[18F]F-p-aminobenzoic acid detects *Staphylococcus aureus* infections and monitors drug response. ACS Infect Dis **2018**; 4:1635–44.
37. Li Y, Daryaee F, Yoon GE, et al. Positron emission tomography imaging of *Staphylococcus aureus* infection using a nitro-prodrug analogue of 2-[18F]F-p-aminobenzoic acid. ACS Infect Dis **2020**; 6:2249–59.
38. Huang L, Fang J, Hong S, et al. MicroPET imaging of bacterial infection with nitroreductase-specific responsive 18F-labelled nitrogen mustard analogues. Eur J Nucl Med Mol Imaging **2022**; 49:2645–54.
39. Petrik M, Umlaufova E, Raclavsky V, et al. 68Ga-labelled desferrioxamine-B for bacterial infection imaging. Eur J Nucl Med Mol Imaging **2021**; 48:372–82.
40. Jiang H, Gu J, Zhao H, et al. PET study of sphingosine-1-phosphate receptor 1 expression in response to *S. aureus* infection. Mol Imaging **2021**; 2021:1–11.
41. Mills B, Awais RO, Luckett J, et al. [(18)F]FDG-6-P as a novel in vivo tool for imaging staphylococcal infections. EJNMMI Res **2015**; 5.
42. Akhtar MS, Iqbal J, Khan MA, et al. 99mTc-labeled antimicrobial peptide ubiquicidin (29–41) accumulates less in *Escherichia coli* infection than in *Staphylococcus aureus* infection. J Nucl Med **2004**; 45:849–56.
43. Afzelius P, Nielsen OL, Alstrup AK, et al. Biodistribution of the radionuclides (18)F-FDG, (11)C-methionine, (11) C-PK11195, and (68)Ga-citrate in domestic juvenile female pigs and morphological and molecular imaging of the tracers in hematogenously disseminated *Staphylococcus aureus* lesions. Am J Nucl Med Mol Imaging **2016**; 6:42–58.
44. Afzelius P, Alstrup AKO, Nielsen OL, Nielsen KM, Jensen SB. Attempts to target *Staphylococcus aureus* induced osteomyelitis bone lesions in a juvenile pig model by using radiotracers. Molecules **2020**; 25.
45. Widerström M. Significance of *Staphylococcus epidermidis* in health care-associated infections, from contaminant to clinically relevant pathogen: this is a wake-up call! J Clin Microbiol **2016**; 54:1679–81.
46. Simpson SR, Kesterson AE, Wilde JH, et al. Imaging diverse pathogenic bacteria in vivo with [18F]fluoromannitol positron emission tomography. J Nucl Med **2022**; 64: 809–15.

47. DeMeester KE, Liang H, Jensen MR, et al. Synthesis of functionalized *N*-acetyl muramic acids to probe bacterial cell wall recycling and biosynthesis. J Am Chem Soc **2018**; 140:9458–65.
48. Peukert C, Langer LNB, Wegener SM, et al. Optimization of artificial siderophores as 68Ga-complexed PET tracers for in vivo imaging of bacterial infections. J Med Chem **2021**; 64:12359–78.